CHAPTER 1

Translational Motion of Water in Biological Tissues – A Brief Primer

D. TOPGAARD

Lund University, Lund, Sweden
Email: daniel.topgaard@fkem1.lu.se

1.1 Introduction

For more than half a century, NMR measurements of the translational motion of water have been used to extract information about porous materials on the microscopic scale.[1–3] Today, by far the largest application of the method is in clinical MRI for assessment of, *e.g.*, stroke[4,5] and cancer.[6–9] The MRI results are conventionally reported in terms of apparent diffusion coefficients (ADCs) which have been related to tissue properties such as cell densities and membrane permeabilities.[10,11] When using NMR to study complex heterogeneous materials like biological tissues, it is useful to decompose the overall translational motion into short-time diffusivity,[12] restriction,[1] anisotropy,[2,13] flow,[14] and exchange,[15] as well as to correlate the translational motion with other NMR observables such as nuclear relaxation rates[16] that report on the local chemical composition of the aqueous phase. This book deals with MRI implementations of advanced diffusion encoding methods targeting these specific aspects of translational motion.[17–22] Before going into the detailed descriptions of the methods in Chapters 2–7, this chapter will give a brief non-mathematical primer on the basic relations between tissue properties and the translational motion of the tissue water.

New Developments in NMR No. 24
Advanced Diffusion Encoding Methods in MRI
Edited by Daniel Topgaard

Published by the Royal Society of Chemistry, www.rsc.org

The outline of this chapter is as follows. First, computer simulations are used to illustrate the molecular-level influence of biomembranes and macromolecules on water dynamics. Subsequently, experimental data from biologically relevant model systems show the effects of these structures on water diffusion on the micrometer length scales relevant for diffusion MRI. Finally, finite element calculations are used to visualize the relations between cell and tissue properties and the specific aspects of the water displacement patterns that can be assessed with the advanced diffusion encoding methods.

1.2 A Molecular Perspective on Water Diffusion in Biological Tissues

MRI monitors translational motion on millisecond time scales and micrometer length scales, which are several orders of magnitude larger than the molecular scales. Still, it is instructive to first assume a molecular perspective on diffusion in order to build an understanding of the relevant factors for explaining experimental observations on the much larger scales defined by MRI. From the perspective of water diffusion, biological tissue can be seen as an ‘‘obstacle course’’ formed by tightly packed assemblies of cells filled with and surrounded by macromolecules such as proteins, nucleic acids, and carbohydrates, and with outer boundaries defined by biomembranes comprising lipids, proteins, and cytoskeleton.

1.2.1 Biomembranes

The influence of biomembranes on water motion can be gleaned from the molecular dynamics simulation[23] in Figure 1.1 focusing on the lipid components which spontaneously assemble into bilayers with minimal contact between the hydrophobic tails and the water. The simulation was carried out by defining initial atom positions consistent with experimental data for average bilayer thickness and lipid–lipid in-plane distance, drawing atom velocities from a distribution corresponding to a temperature of 298 K, and letting the system evolve deterministically according to Newton's laws of motion with a time-step of 2 fs and a total evolution time approaching 1 μs.[24,25] The output of the simulation is a time-resolved series of atom coordinates, velocities, and forces, from which a wide range of structural, dynamic, and thermodynamic properties can be derived for validation against experimental data.

Figure 1.1 shows the final configuration of the simulation overlain with a 50 ns trajectory of a single hydrogen atom on a water molecule. During this time, the water molecule has repeatedly traversed the 5 nm gap between the bilayers and made occasional brief excursions into the interiors of the bilayers, consistent with the low but non-zero solubility of water in hydrocarbons.[26] Looking closer at the interface between the water and lipid layers reveals that the water density is decreasing smoothly from the bulk value to nearly zero over a $\sim$1 nm distance, corresponding to 3–4 molecular

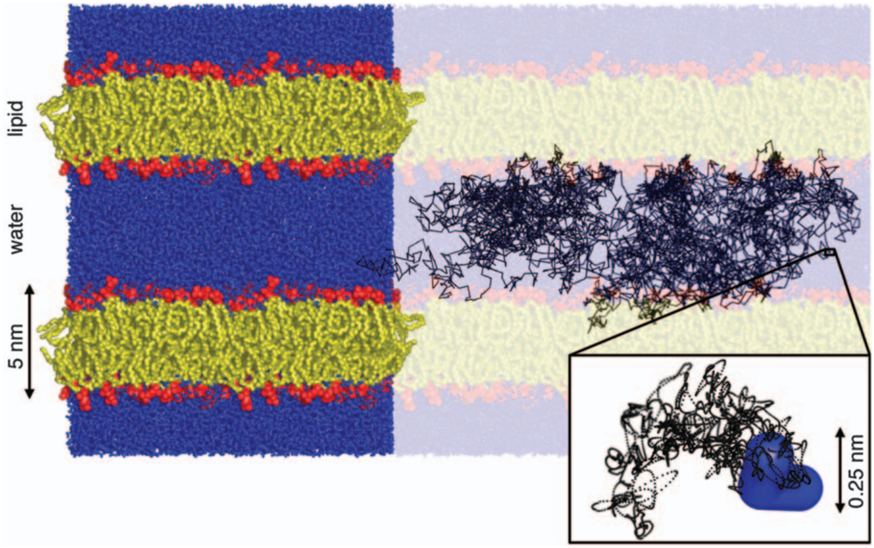

Figure 1.1 Molecular dynamics simulation of a united-atom model of the lipid 1-palmitoyl-2-oleoyl-*sn*-glycero-3-phosphocholine (POPC) at the temperature 298 K, pressure 1 bar, and hydration level 57 water molecules per lipid. The results are shown as a rendering of the final configuration overlain with a 50 ns trajectory of a single water hydrogen sampled at 10 ps intervals (black lines). The lipids are assembled into ~5 nm thick bilayers with the hydrophilic headgroups (red) separating the hydrophobic tails (yellow) from the water (blue). The brightly colored region (left) comprises four replicas of the rectangular simulation box with 128 lipid molecules. The zoom-in (bottom right) shows a 10 ps segment of the hydrogen trajectory at the full 2 fs time resolution of the simulation (black dots) and the final location of the water molecule (blue). (GROMACS[23] simulation results redrawn from ref. 25 using the POV-Ray freeware[60]).

diameters of water. Although not immediately apparent by visual inspection of the figure, quantitative analysis of the simulation data shows a low but finite orientational ordering of the interfacial water,[27] which is readily verified by, *e.g.*, ^{2}H NMR spectroscopy.[28]

The 50 ns trajectory sampled at time-steps of 10 ps may appear as a diffusive random walk with abrupt changes of direction for each step, but it is actually the result of the deterministic motion of a large number of atoms connected into molecules. The zoom-in on a 10 ps segment of the trajectory sampled at each 2 fs time-step of the simulation shows the ballistic regime[29] with a smooth path resulting from the interplay between the velocities and inertias of the individual atoms of the water molecule and the forces from the surrounding atoms on neighboring molecules. The ps-scale reorientational dynamics of water in contact with biomolecules[30,31] and inside bacterial cells[32] and spores[33] has been studied with ^{2}H and ^{17}O NMR relaxation dispersion. For living cells, 85% of the water reorients as rapidly as bulk water (~2 ps correlation time). The remaining 15% that is in direct molecular contact with biomolecules is on average slowed down by a factor of ∼15, which however still yields reorientation on the time scale of a few tens of picoseconds.[32] Correspondingly, quantitative analysis of the simulation trajectories shows that the water molecules during their ∼100 ps brief excursions into the bilayer interfacial region temporarily experience a factor ∼10 reduction in lateral diffusivity compared to bulk water on account of being surrounded by lipids with lateral diffusivity ∼100 times slower than water.[27]

The moderate effects of the lipids on the neighboring water in Figure 1.1 stand in stark contrast to illustrations that occasionally appear in the MRI literature,[34,35] where biomembranes are depicted as covered by perfectly layered and aligned water molecules in support of the ''biphasic model'' of water diffusion in biological tissues.[36–38] As elaborated on by Jungwirth,[39] the notion of highly ordered cell water with properties radically different from conventional liquid water has a long history at the fringes of science and is related to the nowadays discredited theories of water polymerization and ''memory'' of previous contacts with solutes.

Although the lipid membranes have negligible influence on the molecular-scale water dynamics beyond direct molecular contact, the low water concentration in the bilayer interior means that the membranes are efficient barriers for long-range water diffusion. The low permeability is manifested as low water diffusivities as measured with conventional diffusion NMR across macroscopically ordered stacks of hydrated lipid membranes[40] or in foam-like emulsions where the membranes divide the water into discrete compartments with <1 μm radius.[41]

1.2.2 Macromolecules

The crowded interior of a living cell is nicely illustrated with the configuration from a Brownian dynamics simulation of intracellular macromolecules in Figure 1.2 by McGuffee *et al.*[42] To make the simulation model computationally feasible, it focuses on the main protein and RNA components but excludes lipids, DNA, and carbohydrates, and treats water and other small molecules and ions as a continuous medium over which the macromolecules interact while performing random walks with displacements chosen according to stochastic rules.[43] Although the space appears filled with macromolecules, ∼80% of the volume is still available for the aqueous solution through which the water molecules can readily diffuse by simply going around and between the macromolecular obstacles. Theoretical models for the reduction in diffusivity of the small molecules as a function of the volume fraction, shape, and packing pattern of the obstructing objects can be found in the literature.[44–48]

For large differences in size between the solvent and solute molecules, the diffusion of the small molecules is decoupled from that of the large ones. On account of jamming, concentrated systems of colloidal particles may have a solid-like macroscopic appearance while the diffusion of the interstitial water molecules is only marginally reduced from that of pure water.[49]

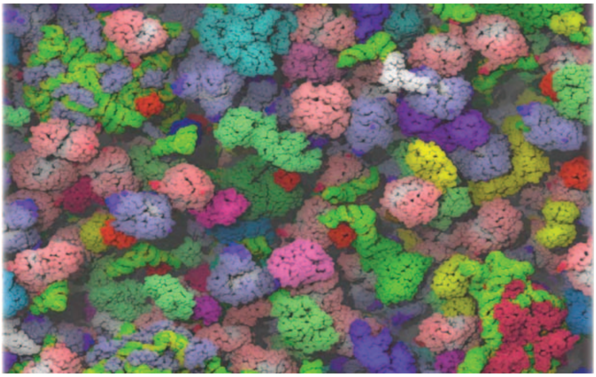

Figure 1.2 Snapshot from a Brownian dynamics simulation of selected macromolecules in the bacterial cytoplasm. RNA (green and yellow) and proteins (other colors) together occupy 20% of the volume. The globular proteins have diameters of ∼5 nm. Water and other small molecules and ions are implicitly included in the simulation model as a continuous medium over which the macromolecules interact.
Adapted from ref. 42, https://doi.org/10.1371/journal.pcbi.1000694 under the terms of the CC BY 4.0 licence, https://creativecommons.org/licenses/by/4.0/.

The macroscopic viscosity of a substance such as a polymer gel or colloidal suspension is thus a poor predictor of the diffusivity of small molecules in a continuous phase between the macromolecules or particles.

1.3 Experimental Data on Biomembrane Permeability and Macromolecular Obstruction

Within physical chemistry, biophysics, and colloid science, there is a large body of literature dealing with the influence of macromolecules and lipid membranes on water dynamics. With the risk of losing some of the biological relevance, these studies are often performed on simple model systems amenable to molecular-level interpretations and direct comparison between experimental results and theoretical approaches such as mean-field calculations or computer simulations like the ones in Figure 1.1 and Figure 1.2. Some selected experimental data on the influence of membranes and macromolecules on water diffusion are shown in Figure 1.3. The barrier properties of the membranes are reported in terms of the diffusive permeability for a series of phospholipids as a function of temperature.[50] At the chain-melting temperature, the acyl chains undergo a transition from a liquid state with a range of *gauche* and *trans* conformations, as in Figure 1.1, to a solid state with closely packed all-*trans* chains, leading to a dramatic drop in permeability. Temperature-dependent permeability data for the plasma membrane of baker's yeast resemble the values and trends for the liquid-state phospholipids,[51] whereas the red blood cells have more than ten times higher permeability on account of their abundance of water channel

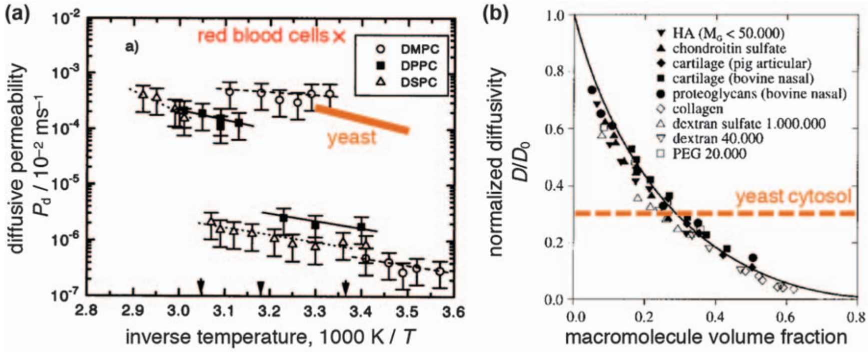

Figure 1.3 Effects of biomembranes and macromolecules on the translational motion of water. (a) Diffusive permeability P_d as a function of inverse temperature $1/T$ for water traversing biomembranes comprising pure phosphatidylcholine lipids with saturated acyl chains of varying lengths (DMPC, DPPC, and DSPC: 14, 16, and 18 carbons), as well as for the plasma membranes of red blood cells (red cross at 298 K)[52] and baker's yeast (orange solid line in the range 286–303 K).[51] Arrowheads along the abscissa indicate the acyl chain melting temperatures at which the permeability abruptly changes by two orders of magnitude for the pure lipids. Adapted from ref. 50 with permission from the Biophysical Society, Copyright 1995. (b) Water diffusivity D at 293 K normalized by the value for bulk water D_0 as a function of macromolecule volume fraction for aqueous solution of a wide range of biological and synthetic polymers as reported in the legend (symbols). The data points fall on a master curve (solid line) calculated with the Mackie and Meares model.[44] The value for water in the cytosol of baker's yeast (orange dashed line) is consistent with a macromolecule volume fraction of 0.3.[57] Adapted from ref. 56 with permission from John Wiley and Sons, Copyright © 1999 Wiley-Liss, Inc.

proteins.[52,53] Such high membrane permeability can also be found in yeast strains genetically modified to express channel proteins.[54,55]

The enormous range of membrane permeabilities for the biologically relevant systems in Figure 1.3 leads to ambiguities when attempting to interpret *in vivo* diffusion MRI data in terms of microstructural properties. On the 100 ms time scale of diffusion MRI experiments and for typical cell sizes, the solid-state lipids are impassable barriers that trap the water molecules within their initial cell, the red blood cell membrane is just a minor obstacle that can easily be penetrated, and the liquid-state lipids and (non-modified) yeast membrane are something in-between: rather good barriers allowing a significant fraction of the water molecules to escape. In much of the diffusion MRI literature, the conventional ADC metric is often interpreted as a proxy for cell density,[6–9] but could just as well be attributed to membrane permeability determined by the details of the chemical composition or physical state of the lipids, or the concentration of channel proteins. Contrary to physical properties such as the self-diffusion coefficient of water, it is very difficult to predict even the correct order of magnitude of the plasma membrane permeability for a given cell type.

In comparison to membrane permeabilities, the influence of macromolecules on water diffusivity is easier to predict as shown in Figure 1.3(b).[56] For a range of biological and synthetic polymers, the water diffusivity *versus* macromolecule volume fraction follows a master curve predicted by the Mackie and Meares model.[44] The diffusivity of intracellular water in yeast has been measured to ∼30% of the value for bulk water,[57] which according to the experimental data in Figure 1.3(b) corresponds to a macromolecule volume fraction of ∼30%. In addition to macromolecules, the measured obstruction effect in yeast includes contributions from the multitude of biomembrane structures within the cell, for instance in the nucleus, mitochondria, and endoplasmic reticulum, which in general contain channel proteins facilitating the passage of water.

1.4 Diffusivity, Restriction, Anisotropy, Exchange, and Flow

Taken together, the results in the previous section suggest the following simple approach for rationalizing water diffusion in biological tissues on the time and length scales relevant for diffusion MRI. The effects of all submicrometer objects such as macromolecules and permeable intracellular membranes can be lumped into a general reduction in water diffusivity that nevertheless may vary between different cell types depending on the chemical composition. More dramatic effects on water diffusion originate from the potentially impermeable biomembranes that form structures on the micrometer length scales defined by the diffusion MRI measurement processes.

Figure 1.4 shows schematic arrangements of membranes in biological tissues and how they affect the translational motion of water molecules. The water motion is visualized by imagining that we "paint" the molecules within a sub-micrometer volume and follow how they spread out with time. On the length scale of the cells, we are not able to resolve individual molecules, as in Figure 1.1, but instead see an "ink spot" giving their concentration (number per unit volume) as a function of position and time. The evolution of the ink spots in Figure 1.4 was calculated with a finite element approach wherein Fick's second law of diffusion is solved on a grid of spatial positions with different local diffusivities and equilibrium concentrations.[58,59] At the shortest time, the ink spots for all cases (a)–(f) are identical and completely determined by the local water diffusivity, while at longer times, the sizes, shapes, and orientations of the spots are given by an interplay between the tendency to spread out by molecular diffusion, the geometrical arrangements and permeabilities of the barriers formed by the biomembranes, and, for case (f), the presence of flow in a single direction. For free diffusion without barriers in (a), the labelled water molecules spread out in an isotropic Gaussian pattern with "size" given by the root-mean-square displacement which increases as the square-root of time. The impermeable barriers in (a), (b), and (c) prevent the labelled molecules from exiting their initial cells, and, in the limit of long times, the spots assume the sizes,

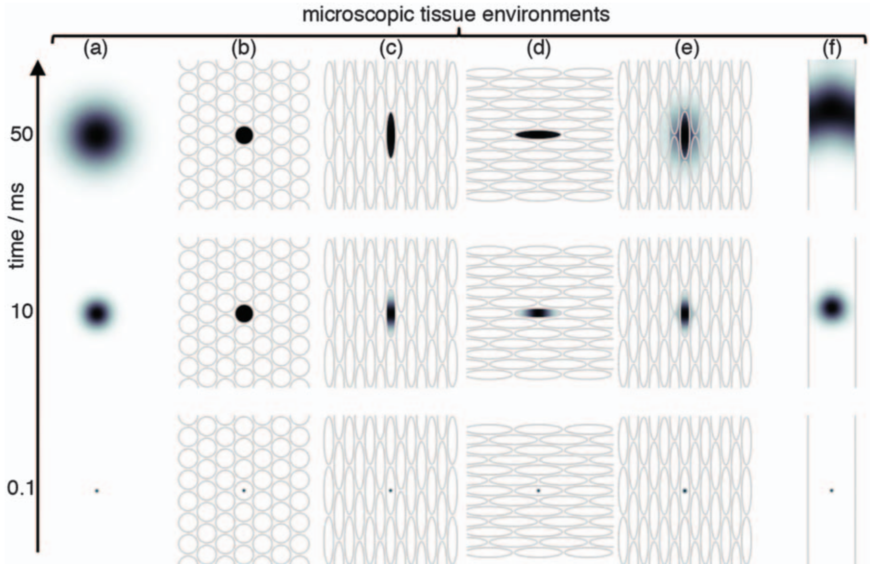

Figure 1.4 Illustration of the distinct phenomena of short-time diffusivity, restriction, anisotropy, exchange, and flow that all occur in living biological tissues and may be independently and unambiguously interrogated with appropriately designed advanced diffusion encoding methods (see Chapters 2–7). The short-time diffusivity is determined by the local chemical composition of the aqueous phase and biomembranes (grey lines) influence the evolution (bottom to top) of the diffusion propagators ("ink spots") on the millisecond time scales and micrometer length scales relevant for diffusion MRI. The sizes, shapes, and orientations of the spots are intuitively related to the underlying tissue properties. (a) Free diffusion in pure water with diffusivity $3.0 \cdot 10^{-9}$ $m^2 s^{-1}$ at 37 °C giving isotropic root-mean-square displacements of 0.77, 7.7, and 17 μm during the times 0.1, 10, and 50 ms. (b) Isotropic tissue with densely packed spherical cells restricting the size of the spot while preserving its spherical shape. (c) Anisotropic tissue with orientationally ordered elongated cells limiting water motion mainly in the horizontal direction. (d) Elongated cells limiting water motion in the vertical direction. (e) Finite membrane permeability allowing the molecules to exchange between the intra- and extracellular spaces. (f) Laminar flow with parabolic velocity profile superposed on the diffusion.

shapes, and orientations of the cells. The finite permeabilities of the membranes in (e) permits molecular exchange between the intra- and extracellular spaces and leads to less sharp relations between the cell and spot geometries. Still, the general shapes and orientations of the cells are imprinted on the corresponding properties of the spots, while the cell density and membrane permeability influence the spot size. The final case in (f) highlights the combined effects of diffusion and steady flow with a parabolic profile as would result from applying a pressure difference to a fluid in a cylindrical pipe, which can be taken as a very crude model of the action of the pumping heart on the blood in the vessels.

The cases in Figure 1.4 are selected to illustrate relevant aspects of water translational motion in biological tissues that can be targeted with advanced diffusion MRI. Removing the influence of the plasma membranes and focusing on the effects of intracellular obstacles such as macromolecules requires reducing the observational time scale to below 1 ms. At longer times, the influence of the micrometer scale geometries of the biomembranes and their barrier properties become noticeable. Whereas adjustment of the measurement direction gives information about compartment shapes and orientations (Chapter 3), systematic variation of the time scales of the measurement process gives access to several relevant properties such as the spacings between biomembrane barriers (Chapter 4), flow velocities in the microcapillary network (Chapter 5), and the rates of molecular exchange over cell membranes and between regions with distinct local diffusion properties (Chapter 6).

1.5 Summary

This chapter has summarized the aspects of water diffusion in biological tissues that may be interrogated with advanced diffusion MRI methods. On the molecular time and length scales of nanoseconds and nanometers, biomolecules such as lipids, proteins, and nucleic acids impart a weak alignment and moderate slowing down of the reorientational and translational motion of the immediately neighboring water molecules. The dimensions of macromolecules and intracellular biomembranes are orders of magnitude smaller than the displacements probed by diffusion MRI, and thus mainly contribute with a modest lowering of the water diffusivity in comparison to the value for bulk water. More dramatic effects originate from the plasma membranes that, depending on the chemical composition and concentration of channel proteins, may present formidable barriers for the water molecules on the micrometer length scales and millisecond time scales defined by the measurement process in diffusion MRI. The effects of the geometries and barrier properties of the membranes on the translational motion of the water can be visualized as the spreading out of ‘‘ink spots’’, whose sizes, shapes, and orientations are intuitively related to the underlying structures.

Acknowledgements

This work was financially supported by the Swedish Foundation for Strategic Research (ITM17-0267) and the Swedish Research Council (2018-03697).

References

1. D. E. Woessner, *J. Phys. Chem.*, 1963, **67**, 1365.
2. B. D. Boss and E. O. Stejskal, *J. Chem. Phys.*, 1965, **43**, 1068.
3. J. E. Tanner and E. O. Stejskal, *J. Chem. Phys.*, 1968, **49**, 1768.
4. M. E. Moseley, K. Butts, M. A. Yenari, M. Marks and A. de Crespigny, *NMR Biomed.*, 1995, **8**, 387.

5. H. L. Lutsep, G. W. Albers, A. DeCrespigny, G. N. Kamat, M. P. Marks and M. E. Moseley, *Ann. Neurol.*, 1997, **41**, 574.
6. A. R. Padhani, G. Liu, D. Mu-Koh, T. L. Chenevert, H. C. Thoeny, T. Takahara, A. Dzik-Jurasz, B. D. Ross, M. Van Cauteren, D. Collins, D. A. Hammoud, G. J. S. Rustin, B. Taouli and P. L. Choyke, *Neoplasia*, 2009, **11**, 102.
7. J. O. Barentsz, J. C. Weinreb, S. Verma, H. C. Thoeny, C. M. Tempany, F. Shtern, A. R. Padhani, D. Margolis, K. J. Macura, M. A. Haider, F. Cornud and P. L. Choyke, *Eur. Urol.*, 2016, **69**, 41.
8. P. Baltzer, R. M. Mann, M. Iima, E. E. Sigmund, P. Clauser, F. J. Gilbert, L. Martincich, S. C. Partridge, A. Patterson, K. Pinker, F. Thibault, J. Camps-Herrero and D. Le Bihan, *Eur. Radiol.*, 2020, **30**, 1436.
9. J. Camps-Herrero, *BJR|Open*, 2019, **1**, 20180049.
10. C. Beaulieu, *NMR Biomed.*, 2002, **15**, 435.
11. D. Le Bihan, *Nat. Rev. Neurosci.*, 2003, **4**, 469.
12. J. E. Tanner, *Biophys. J.*, 1979, **28**, 107.
13. D. G. Cory, A. N. Garroway and J. B. Miller, *Polym. Prepr.*, 1990, **31**, 149.
14. H. Y. Carr and E. M. Purcell, *Phys. Rev.*, 1954, **94**, 630.
15. J. Kärger, *Ann. Phys.*, 1969, **479**, 1.
16. D. van Dusschoten, P. A. de Jager and H. Van As, *J. Magn. Reson., Ser. A*, 1995, **116**, 22.
17. C. B. Ahn, S. Y. Lee, O. Nalcioglu and Z. H. Cho, *Med. Phys.*, 1987, **14**, 43.
18. S. Mori and P. C. M. van Zijl, *Magn. Reson. Med.*, 1995, **33**, 41.
19. M. Lawrenz and J. Finsterbusch, *Magn. Reson. Med.*, 2011, **66**, 1405.
20. M. Nilsson, J. Lätt, D. van Westen, S. Brockstedt, S. Lasič, F. Ståhlberg and D. Topgaard, *Magn. Reson. Med.*, 2013, **69**, 1573.
21. C. A. Baron and C. Beaulieu, *Magn. Reson. Med.*, 2014, **72**, 726.
22. F. Szczepankiewicz, S. Lasič, D. van Westen, P. C. Sundgren, E. Englund, C.-F. Westin, F. Ståhlberg, J. Lätt, D. Topgaard and M. Nilsson, *NeuroImage*, 2015, **104**, 241.
23. D. van der Spoel, E. Lindahl, B. Hess, G. Groenhof, A. E. Mark and H. J. Berendsen, *J. Comput. Chem.*, 2005, **26**, 1701.
24. T. M. Ferreira, F. Coreta-Gomes, O. H. S. Ollila, M. J. Moreno, W. L. C. Vaz and D. Topgaard, *Phys. Chem. Chem. Phys.*, 2013, **15**, 1976.
25. T. M. Ferreira, O. H. S. Ollila, R. Pigliapochi, A. P. Dabkowska and D. Topgaard, *J. Chem. Phys.*, 2015, **142**, 044905.
26. C. Black, G. G. Joris and H. S. Taylor, *J. Chem. Phys.*, 1948, **16**, 537.
27. K. Åman, E. Lindahl, O. Edholm, P. Håkansson and P.-O. Westlund, *Biophys. J.*, 2003, **84**, 102.
28. J. Ulmius, H. Wennerström, G. Lindblom and G. Arvidson, *Biochemistry*, 1977, **16**, 5742.
29. P. N. Pusey, *Science*, 2011, **332**, 802.
30. B. Halle, T. Andersson, S. Forsén and B. Lindman, *J. Am. Chem. Soc.*, 1981, **103**, 500.
31. B. Halle and H. Wennerström, *J. Chem. Phys.*, 1981, **75**, 1928.
32. E. Persson and B. Halle, *Proc. Natl. Acad. Sci. U. S. A.*, 2008, **105**, 6266.

33. E. P. Sunde, P. Setlow, L. Hederstedt and B. Halle, *Proc. Natl. Acad. Sci. U. S. A.*, 2009, **106**, 19334.
34. D. Le Bihan, *Phys. Med. Biol.*, 2007, **52**, R57.
35. D. Le Bihan, in *Water: The Forgotten Biomolecule*, ed. D. Le Bihan and H. Fukuyama, Pan Stanford Publishing Pte. Ltd., 2011.
36. D. Le Bihan, S. Urayama, T. Aso, T. Hanakawa and H. Fukuyama, *Proc. Natl. Acad. Sci. U. S. A.*, 2006, **103**, 8263.
37. C. J. Galbán, B. A. Hoff, T. L. Chenevert and B. D. Ross, *NMR Biomed.*, 2017, **30**, e3458.
38. D. K. Jones, D. C. Alexander, R. Bowtell, M. Cercignani, F. Dell'Acqua, D. J. McHugh, K. L. Miller, M. Palombo, G. J. M. Parker, U. S. Rudrapatna and C. M. W. Tax, *NeuroImage*, 2018, **182**, 8.
39. P. Jungwirth, *Nature*, 2011, **474**, 168.
40. P. Wästerby, G. Orädd and G. Lindblom, *J. Magn. Reson.*, 2002, **157**, 156.
41. D. Topgaard, C. Malmborg and O. Söderman, *J. Magn. Reson.*, 2002, **156**, 195.
42. S. R. McGuffee and A. H. Elcock, *PLoS Comput. Biol.*, 2010, **6**, 1.
43. D. L. Ermak and H. Buckholz, *J. Comput. Phys.*, 1980, **35**, 169.
44. J. S. Mackie and P. Meares, *Proc. Math. Phys. Eng. Sci.*, 1955, **232**, 498.
45. B. Jönsson, H. Wennerström, P. G. Nilsson and P. Linse, *Colloid Polym. Sci.*, 1986, **264**, 77.
46. L. L. Latour, K. Svoboda, P. P. Mitra and C. H. Sotak, *Proc. Natl. Acad. Sci. U. S. A.*, 1994, **91**, 1229.
47. K.-J. Dunn and D. J. Bergman, *J. Chem. Phys.*, 1995, **102**, 3041.
48. H. Jóhannesson and B. Halle, *J. Chem. Phys.*, 1996, **104**, 6807.
49. A. Svensson, D. Topgaard, L. Piculell and O. Söderman, *J. Phys. Chem. B*, 2003, **107**, 13241.
50. M. Jansen and A. Blume, *Biophys. J.*, 1995, **68**, 997.
51. I. Åslund, A. Nowacka, M. Nilsson and D. Topgaard, *J. Magn. Reson.*, 2009, **200**, 291.
52. R. Ye and A. S. Verkman, *Biochemistry*, 1989, **28**, 824.
53. P. Agre, *Angew. Chem., Int. Ed.*, 2004, **43**, 4278.
54. S. Eriksson, K. Elbing, O. Söderman, K. Lindkvist-Petersson, D. Topgaard and S. Lasič, *PLoS One*, 2017, **12**, e0177273.
55. M. Palmgren, M. Hernebring, S. Eriksson, K. Elbing, C. Geijer, S. Lasič, P. Dahl, J. S. Hansen, D. Topgaard and K. Lindkvist-Petersson, *J. Membr. Biol.*, 2017, **250**, 629.
56. R. Knauss, J. Schiller, G. Fleischer, J. Kärger and K. Arnold, *Magn. Reson. Med.*, 1999, **41**, 285.
57. I. Åslund and D. Topgaard, *J. Magn. Reson.*, 2009, **201**, 250.
58. H. Hagslätt, B. Jönsson, M. Nydén and O. Söderman, *J. Magn. Reson.*, 2003, **161**, 138.
59. S. N. Hwang, C.-L. Chin, F. W. Wehrli and D. B. Hackney, *Magn. Reson. Med.*, 2003, **50**, 373.
60. POV-Ray 3.7, www.povray.org.